RESEARCH ARTICLE
doi: 10.2306/scienceasia1513-1874.2026.067

ScienceAsia 52 (4): 2026: ID 2026067: **1–8**

Enhancing the desalination performance of thin-film composite membranes by suppressing interfacial defects between UiO-66-2 NH_2 and the polyamide matrix

Qiang Huang[a], Hao Sun[a,*], Hongshuai Yu[b], Pengwei Zhang[a], Jinquan Wang[a], Yazhou Kong[a], Fei Liu[a,*]

[a] National & Local Joint Engineering Research Center for Mineral Salt Deep Utilization, School of Chemical Engineering, Huai'an University, Huaian 223003 China
[b] Qingdao Jin Yuan Environmental Engineering Co., Ltd., Qingdao 266000 China

*Corresponding authors, e-mail: huangongsun_hao@163.com, liufei@hyit.edu.cn

Received 28 Jan 2026, Accepted 22 Jun 2026
Available online 19 Jul 2026

ABSTRACT: Incorporating nanoporous materials into polyamide rejection layers is a well-established strategy for enhancing the permeability of thin-film composite (TFC) membranes. However, interfacial defects between the nanomaterials and the polyamide matrix often undermine membrane selectivity. In this study, UiO-66-2 NH_2 nanoparticles were synthesized and incorporated into TFC membranes. The optimized integration of UiO-66-2 NH_2 into the polyamide layer significantly increased the membrane permeability to 3.40 l/m^2/h/bar, while simultaneously improving the salt rejection from 97.6% to 99.0%. The increased permeability of TFC membranes could be attributed to the abundant nanochannels present within the embedded UiO-66-2 NH_2 particles. Additionally, the high-density amine groups on UiO-66-2 NH_2 surface reacted with trimesoyl chloride (TMC), effectively suppressing defect formation at the interface.

KEYWORDS: UiO-66-2 NH_2, TFC membrane, interfacial defects

INTRODUCTION

The critical importance of clean water provision for human livelihood and economic sustainability necessitates the advancement of water purification technologies capable of treating both conventional and non-conventional water resources [1, 2]. Reverse osmosis (RO) membrane technology has emerged as the predominant global solution for seawater desalination and water purification, driven by its operational simplicity and energy-efficient separation mechanism [3–5]. Nevertheless, the development of RO membranes faces inherent limitations due to the fundamental trade-off between membrane selectivity and permeability [6]. The primary challenge lies in achieving enhanced permeability while maintaining robust separation efficiency, a pivotal requirement for optimizing membrane performance in practical applications.

The incorporation of nanoporous materials into polyamide selective layers has been extensively demonstrated as an effective strategy to improve membrane permeability and concurrently alleviating the inherent permeability-selectivity trade-off [7, 8]. Metal-organic framework (MOF), featuring high porosity, uniform pore size, and controllable particle dimensions, has attracted significant attention. Among them, UiO-66 nanoparticles are particularly notable for their high pore density and tunable pore architecture [9, 10]. UiO-66, a zirconium-based MOF constructed from zirconium metal clusters and 1,4-benzenedicarboxylic acid linkers, possesses diverse pore channels with an average diameter around 0.6 nm. Its structural stability in water makes it highly suitable for incorporation into polyamide selective layers to increase water-channel density [11, 12]. To reduce interfacial defects between the polyamide matrix and UiO-66 particles, UiO-66-NH_2—fabricated with 2-aminoterephthalic acid as the organic linker—has emerged as an excellent nanofiller candidate for TFC membranes [13, 14]. Then, Zhao's team confirmed that incorporating UiO-66-NH_2 enhances the permeability of TFC membranes [15]. Liu's team functionalized UiO-66-NH_2 using palmitoyl chloride to enhance its dispersibility in organic solutions [16]. Results indicate that the increase of amino groups within nanoparticles could effectively promote the uniform dispersion of particles within the polyamide layer, reduce the interfacial defects between particles and polyamide macromolecule to maintain high water permeability without compromising salt rejection performance. However, the relatively low density of $-NH_2$ groups in UiO-66-NH_2 results in weak interfacial interaction with the polyamide matrix, thereby offering insufficient suppression of interfacial defects. Consequently, at high filler loadings of UiO-66-NH_2 particles within polyamide layer, severe performance trade-offs emerge—specifically, a pronounced decline in salt rejection—due to compromised membrane integrity and defective nanoscale morphology.

Based on the above phenomenon, in this study, UiO-66-2 NH_2 nanoparticles with double amounts of amino groups than UiO-66-NH_2 nanoparticles were

fabricated and applied to modify TFC membranes. UiO-66-2 NH_2 has a higher $-NH_2$ density than UiO-66-NH_2, enabling robust covalent grafting to the polyamide matrix. This strong interfacial anchoring suppresses nanoscale voids and delamination, allowing higher filler loading without sacrificing performance. As a result, the TFC membrane achieves both higher water permeance and high salt rejection—breaking the permeability—selectivity trade-off. The effect of UiO-66-2 NH_2 loading amount on the morphology and performance of the fabricated UiO-66-2 NH_2/TFC membranes was systematically investigated.

MATERIALS AND METHOD

Materials

Camphorsulfonic acid (CSA, 99%), trimesoyl chloride (TMC, 98%), N,N-dimethylformamide (DMF, 99.5%), n-Hexane (97%), 2-aminoterephthalic acid (H_2BDC-NH_2, 97%), 2,5-diaminoterephthalic acid (H_2DATA, 97%), and dimethyl sulfoxide (DMSO, 99%) were sourced from Aladdin (Shanghai, China). Polyethersulfone (PES) membranes (0.45 μm) were provided by Delvstlab (Haining, China). M-phenylenediamine (MPD, 99%), triethylamine (TEA, 99%), acetic acid (99%), and Zirconium chloride ($ZrCl_4$, 98%) were purchased from Shanghai Meryer (Shanghai, China). Sodium dodecyl sulfate (SDS, 98%) was acquired from Shanghai Macklin (Shanghai, China).

Fabrication of UiO-66-2 NH_2 nanoparticles and TFC membranes

First, $ZrCl_4$ (0.4 mmol), H_2DATA (0.4 mmol), 46 ml DMF and 6 ml acetic acid were mixed and stirred in the 150 ml beaker for 30 min. The resulting mixture was poured into the polytetrafluoroethylene-lined autoclave and heated at 120 °C for 24 h. After the reaction, the product was collected via centrifugation at 8000 rpm. The precipitate was separated and washed three times alternately with DMF and anhydrous ethanol. Lastly, the synthesized UiO-66-2 NH_2 material was dried under vacuum at 70 °C for 12 h.

TFC membranes were fabricated using a sequential approach involving pre-deposition followed by interfacial polymerization [17]. First, 0.01 wt% suspensions of UiO-66-2 NH_2 were prepared, after which varying volume of UiO-66-2 NH_2 suspension were deposited onto separate PES membranes (mean pore size: 045 μm, diameter: 5 cm). Subsequently, excess solvent was removed through vacuum filtration. Next, 3 ml of an aqueous solution containing SDS (serves as a surfactant, 0.2 wt%), MPD (2 wt%), TEA (serves as an acid scavenger, 0.5 wt%), DMSO (serves as a co-solvent, 2 wt%), and CSA (serves as a pH regulator, 2 wt%) was applied uniformly across the membrane surface and allowed to reside for 5 min, whereupon excess liquid was removed. Immediately following this, 1.5 ml of an n-hexane solution containing TMC (0.15 wt%) was slowly added to the coated surface. After reacting for 15 min under ambient conditions, the membrane was transferred to a convection oven and dried at 70 °C for 15 min. Finally, the fabricated membrane was stored in deionized water at room temperature.

Membrane characterization

The synthesized nanoparticles and fabricated membranes were analyzed by XRD (XRDynamic-500, Graz, Austria), BET (TriStarll3020, Nocross, USA), FTIR (Nicolet-6700, Madison, USA), SEM-EDS (ZEISS GeminiSEM 300, Oberkochen, Germany), and AFM (Bruker Dimension Icon, Billerica, USA). To evaluate the desalination performance of the membranes, a tangential-flow filtration system equipped with an effective membrane area of 9.07 cm^2 was employed. Membrane permeability and selectivity were determined using a 2000 mg/l NaCl solution under applied pressure of 10 bar at 25 °C. The values for both permeability and selectivity were calculated according to the following equations:

$$J = \frac{\Delta V}{A \times \Delta P \times \Delta t} \quad (1)$$

$$R = \left(\frac{C_i - C_f}{C_i}\right) \times 100\% \quad (2)$$

Here, A (m^2), P (bar), and t (h) represent membrane effective area, operating pressure, duration of the test, respectively. C_f and C_i (mg/l) represent the final and initial concentrations of sodium chloride in the feed and permeate streams, respectively. V (l) represents the volume of the produced permeate water.

RESULTS AND DISCUSSION

Characterization of UiO-66-2 NH_2 nanoparticles

The obtained UiO-66-2 NH_2 nanoparticles exhibit the regular octahedral structure as same as the UiO-66-NH_2 nanoparticles (Fig. 1A,C) [18]. The statistical analysis of particle size distribution indicates that the mean grain size diameter of UiO-66-2 NH_2 particles (88.70 nm) is larger than that of UiO-66-NH_2 particles (79.98 nm) (Fig. 1B,D). The result demonstrates that the increased number of amino groups does not significantly affect the crystal growth, and this phenomenon is consistent with the previous research results.

As shown in the XRD patterns presented in Fig. 2A, the UiO-66-2 NH_2 samples exhibit identical diffraction peaks at 2θ values of 7.4°, 8.5°, 12.0°, 17.0°, 22.2°, and 25.7°, which are assigned to the (111), (002), (022), (004), (115), and (006) crystal planes, respectively. In comparison with UiO-66-NH_2 samples, the corresponding peaks in UiO-66-2 NH_2 samples slightly shift toward the left. This shift is likely due to the higher

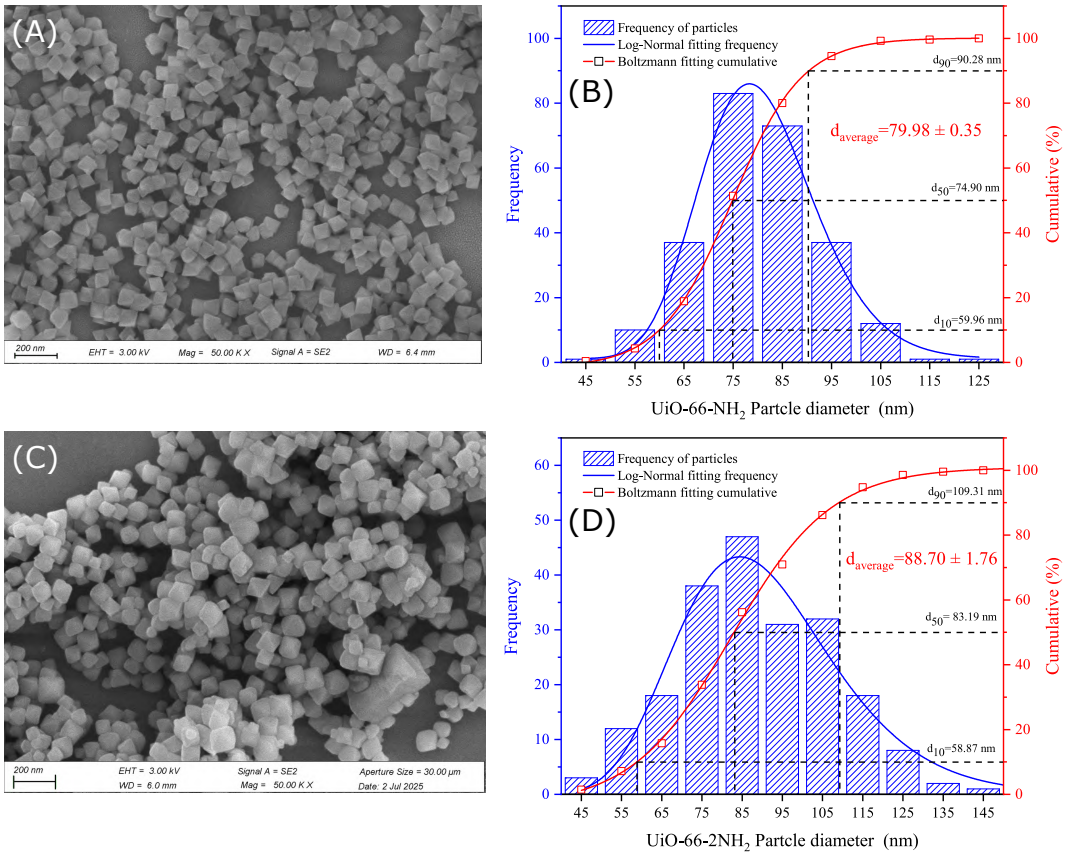

Fig. 1 SEM images and size distributions of UiO-66-NH_2 (A and B) and UiO-66-2 NH_2 (C and D).

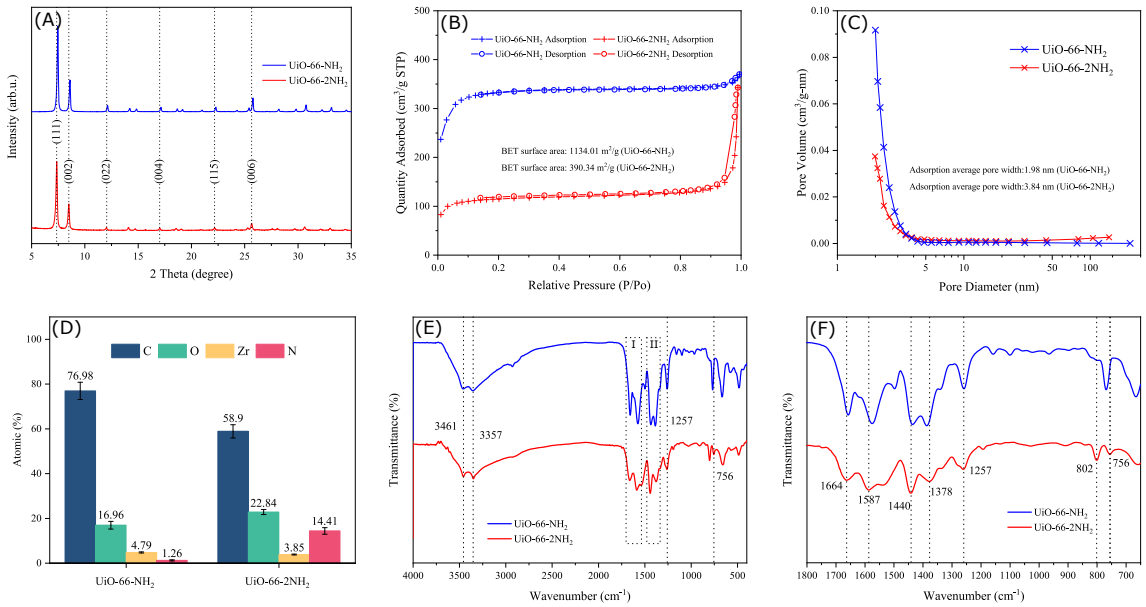

Fig. 2 (A) XRD patterns; (B) N_2 adsorption and desorption isotherms; (C) Pore size distribution; (D) Atomic percentage determined by EDS analysis; (E and F) FTIR spectroscopy.

concentration of amino groups in UiO-66-2 NH_2, which induces lattice expansion [19]. But overall, UiO-66-2 NH_2 samples still retain an analogous crystal structure to its UiO-66-NH_2 crystalline counterparts.

The N_2 adsorption-desorption data in Fig. 2B,C provide quantitative insights into the pore size distribution and specific surface area of the synthesized nanoparticles. UiO-66-2 NH_2 exhibits a specific surface area of 390.34 m^2/g and an intrinsic pore diameter of 3.84 nm, whereas UiO-66-NH_2 demonstrates a higher surface area of 1134.01 m^2/g with a smaller pore size of 1.98 nm. The enlarged pore dimensions of UiO-66-2 NH_2 facilitate improved water permeability in modified TFC membranes relative to those incorporating UiO-66-NH_2, when employed at equivalent loading concentrations.

EDS analysis was employed to examine the elemental composition of the three particle types. As illustrated in Fig. 2D, the nitrogen content increased from 1.26% in UiO-66-NH_2 nanoparticles to 14.41% in UiO-66-2 NH_2 nanoparticles. This result confirms the successful synthesis of UiO-66-2 NH_2. The high density of amino groups present in UiO-66-2 NH_2 particles will significantly enhance the compatibility of nanoparticles within the polyamide macromolecular network [20, 21].

The FTIR spectra of UiO-66-NH_2 and UiO-66-2 NH_2, displayed in Fig. 2E,F, exhibit characteristic peaks near 3461 cm^{-1} and 3357 cm^{-1}, corresponding to the asymmetric and symmetric N—H stretching vibrations, respectively [22, 23]. The presence of aromatic amine groups is further confirmed by the N—H bending vibration near 1664 cm^{-1} and the C—N stretching vibration observed at approximately 1257 cm^{-1} [12, 24]. Additionally, absorption bands at 1587 cm^{-1} and 1378 cm^{-1} are assigned to the asymmetric and symmetric stretching vibrations of carboxylate groups [12, 22]. Peaks at 756 cm^{-1} correspond to the longitudinal and transverse modes of Zr—O [22].

In summary, XRD patterns confirm that the UiO-66-NH_2 framework remains intact after amination, preserving structural integrity for use as a robust porous nanofiller. BET analysis shows a reduced surface area and an increased average pore size-evidence of —NH_2 incorporation into micropores. EDS detects elevated nitrogen content, and FTIR shows clear —NH_2 peaks, confirming successful surface enrichment of amino groups. The abundant —NH_2 groups on UiO-66-2 NH_2 react covalently with TMC or hydrogen-bond with C=O groups in the forming polyamide layer. This dual anchoring improves nanofiller-polymer compatibility, ensuring uniform dispersion and strong integration within the selective layer. As a result, interfacial defects—delamination, voids, and gaps from aggregation—are suppressed, overcoming a major limitation of conventional blended TFC membranes.

Characterization of UiO-66-2 NH_2/TFC membranes

The surface and cross-sectional images of UiO-66-2 NH_2/TFC membranes were shown in Fig. 3. The surface images show the characteristic peak-and-valley features typical of polyamide rejection layers. Besides, no visible UiO-66-2 NH_2 particles or defects were detected on the membrane surfaces. The cross-sectional images reveal that the UiO-66-2 NH_2 particles had been effective encapsulated in the polyamide layers. Furthermore, UiO-66-2 NH_2/polyamide composite rejection layers (M-2 to M-6) are thicker than the conventional polyamide rejection layer (M-1), which can be attributed to that the deposition of UiO-66-2 NH_2 particles on PES membranes enhancing MPD solution uptake and promoting the interfacial polymerization reaction. This successful integration of UiO-66-2 NH_2 into polyamide layers is expected to improve membrane permeability while maintaining its desalination performance.

The AFM images (Fig. 4) were applied to analyze membrane surface roughness. Obviously, the incorporation of UiO-66-2 NH_2 decreased the surface roughness of TFC membranes. With the increase in UiO-66-2 NH_2 loading from 0 g/m^2 (M-1) to 0.704 g/m^2 (M-5), the surface roughness of the membrane declined from 91.5 nm to 73.9 nm. This is attributed to that the hydrophilic UiO-66-2 NH_2 particles could retard the diffusion behavior of aniline, making the interfacial polymerization reaction more mild and suppressing large-scale surface undulations. However, upon further increasing the UiO-66-2 NH_2 loading to increase to 0.880 g/m^2 (M-6), the membrane surface roughness rose to 83.4 nm, likely due to the agglomeration of nanoparticles.

The FTIR spectroscopy of UiO-66-2 NH_2/TFC membranes is presented in Fig. 5. The absorption band at 1668 cm^{-1} corresponds to the amide I band, representing the stretching vibrations of C=O bond [25, 26]. The absorption band at 1540 cm^{-1} was assigned to the amide II band, arising from the C—N stretching and N—H bending vibrations [25]. The peak at 1453 cm^{-1} was likewise attributed to the C—N stretching vibrations [27]. These characteristic amide bands verify the successful formation of polyamide rejection layers in the UiO-66-2 NH_2/TFC membranes. Besides, the peaks around 3353 and 3442 cm^{-1} are assigned to asymmetric and symmetric N—H stretching vibrations respectively, indicative of the NH_2 bond. The peak at 1609 cm^{-1} represents combined N—H deformation and C=C ring stretching vibrations [28]. The peak at 769 cm^{-1} corresponds to the Zr—O bond. Collectively, these spectral features confirm the successful fabrication of a UiO-66-2 NH_2/polyamide composite rejection layer.

As anticipated, the UiO-66-2 NH_2/TFC membranes display reduced water contact angles compared to the pristine TFC membrane, confirming enhanced

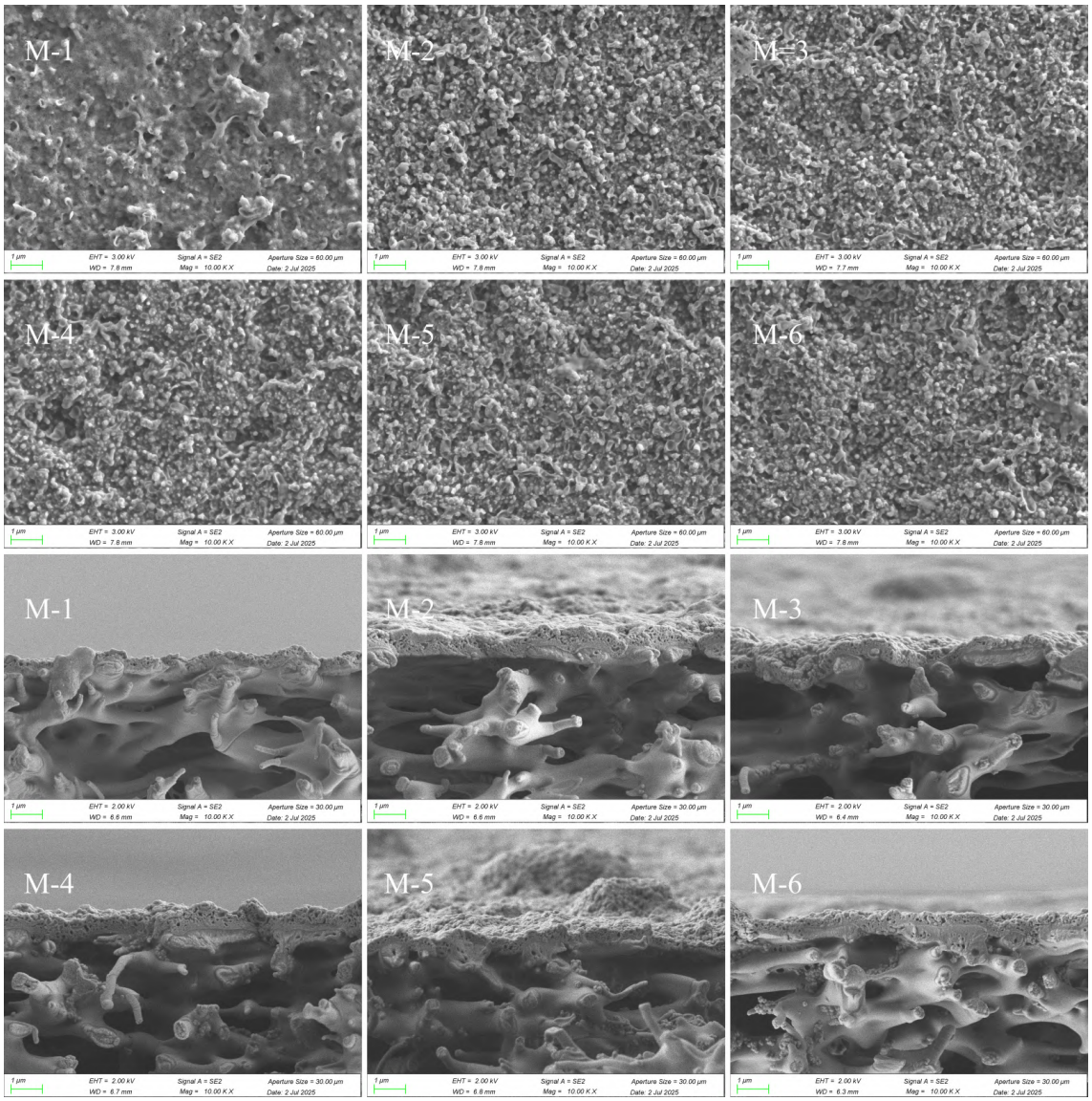

Fig. 3 SEM images of UiO-66-2 NH_2/TFC membranes: (M-1) 0 g/m^2; (M-2) 0.176 g/m^2; (M-3) 0.352 g/m^2; (M-4) 0.528 g/m^2; (M-5) 0.704 g/m^2; (M-6) 0.880 g/m^2.

Table 1 Sample number of the prepared membranes.

Sample	M-1	M-2	M-3	M-4	M-5	M-6
UiO-66-2 NH_2 dispersion solution (ml)	0	2	4	6	8	10
UiO-66-2 NH_2 content (g/m^2)	0	0.176	0.352	0.528	0.704	0.880

surface hydrophilicity upon UiO-66-2 NH_2 incorporation (Fig. 6). As the loading amount of UiO-66-2 NH_2 particles increased from 0 to 0.528 g/m^2, the water contact angles of the UiO-66-2 NH_2/TFC membranes decreased gradually. This result is primarily attributed to the substantial incorporation of hydrophilic amino groups into the membrane matrix and the concurrent reduction in surface roughness, as quantitatively confirmed by AFM. Besides, the M-5 (0.704 g/m^2) and M-6 (0.880 g/m^2) membranes display slightly higher contact angles compared to M-4 (0.528 g/m^2), likely due to adverse effects arising from severe nanoparticle aggregation, as confirmed by cross-sectional SEM images in Fig. 3. In general, this improved surface hydrophilicity is expected to contribute to elevated water flux.

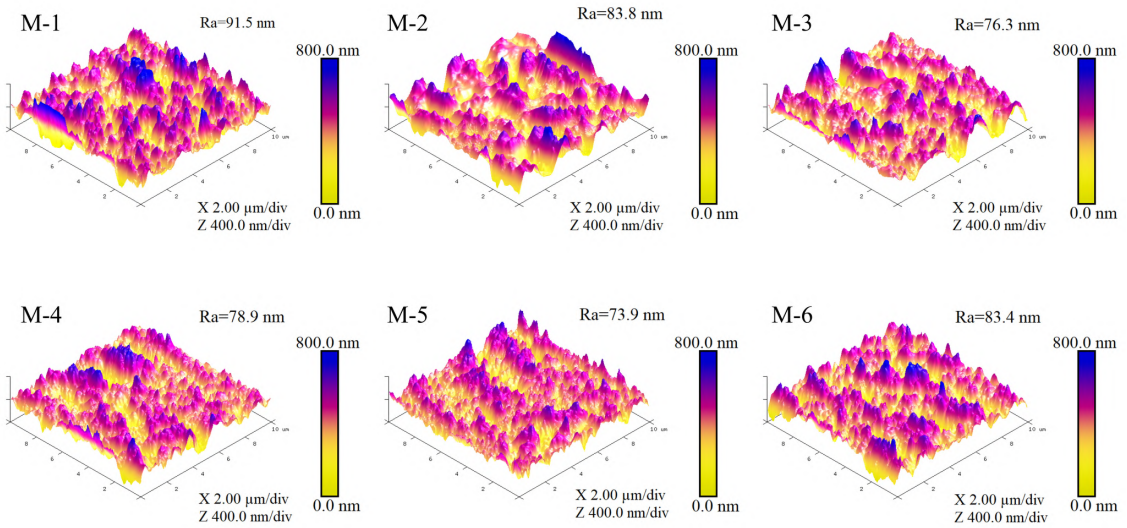

Fig. 4 AFM images of UiO-66-2 NH_2/TFC membranes: (M-1) 0 g/m^2; (M-2) 0.176 g/m^2; (M-3) 0.352 g/m^2; (M-4) 0.528 g/m^2; (M-5) 0.704 g/m^2; (M-6) 0.880 g/m^2.

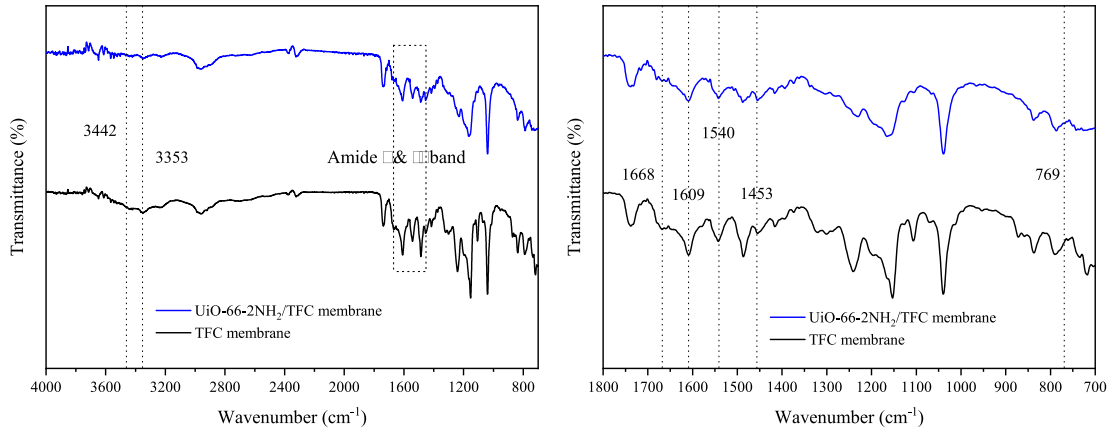

Fig. 5 FTIR spectroscopy of UiO-66-2 NH_2/TFC membranes.

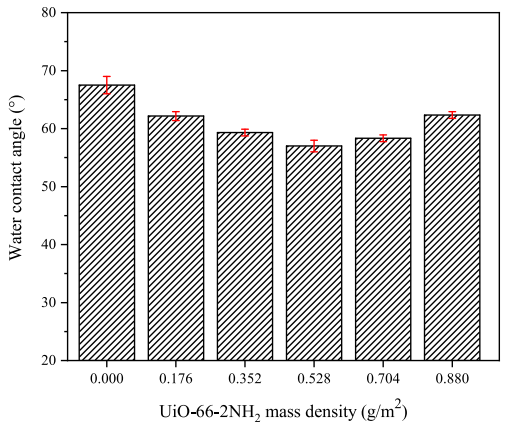

Fig. 6 Contact angle test on the surface of different membranes.

As shown in Fig. 7A, the UiO-66-2 NH_2/TFC membranes demonstrate consistently higher water fluxes in comparison with the unmodified TFC membrane (2.57 l/m^2/h/bar). The water flux exhibits a positive correlation with UiO-66-2 NH_2 loading within an optimal range, whereas excessive particle loading gradually reduces water permeation. Specifically, the M-4 (0.528 g/m^2) membrane achieves a water flux of 3.40 l/m^2/h/bar, representing a 32.3% enhancement over the pristine TFC membrane. These improvements originate from two fundamental characteristics of the MOF material: (1) its hydrophilic surface chemistry, conferred by amine (—NH_2) functional groups grafted onto the UiO-66 framework, promotes strong hydrogen bonding with water molecules, thereby reducing interfacial resistance and accelerating surface hydration; (2) its well-defined intrinsic microporosity, intrinsic microporosity serves as additional, low-resistance transport pathways for water molecules across the

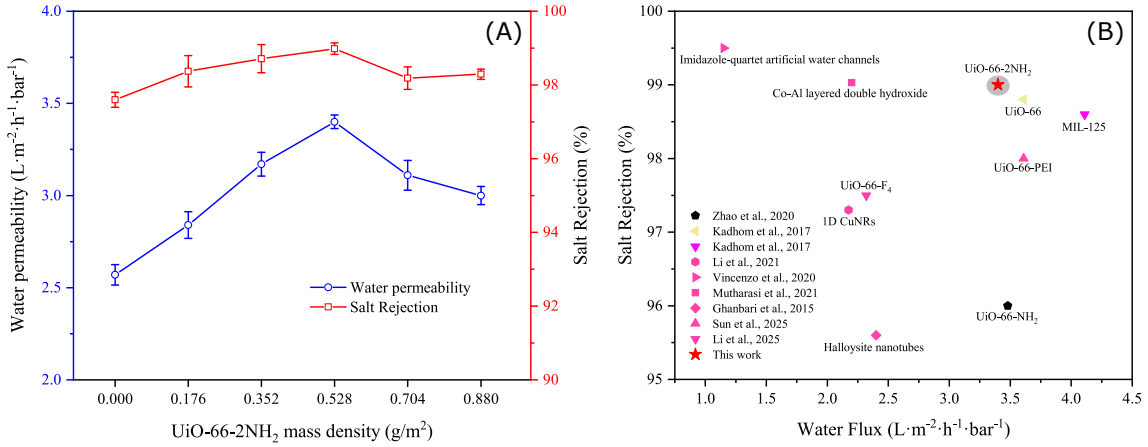

Fig. 7 Separation performance for (A) UiO-66-2 NH_2/TFC membranes and (B) other water channel TFC membranes [15, 29, 30].

membrane. Beyond the optimal loading, the water flux of membranes showed a little decrease due to the severe nanoparticle aggregation and the greater mass transfer resistance caused by the increase in the thickness of the separation layer, as confirmed by cross-sectional SEM images in Fig. 3. The membrane desalination performance follows a similar trend: M-4 (0.528 g/m^2) membrane achieves 99.0% rejection, surpassing the 97.6% rejection of the pristine TFC membrane. This indicates complete encapsulation of MOFs by the formed polyamide layer, thereby well-maintained salt rejection. Besides, as shown in Fig. 7B, the reported TFC RO membranes are limited by the trade-off effect, resulting to the decrease of desalination performance while increasing its permeability performance. In this study, the high density of amine groups on UiO-66-2 NH_2 enables two key interactions during polyamide formation: covalent amidation with TMC and hydrogen bonding with C=O groups in the polyamide network. This dual anchoring improves nanofiller-polymer compatibility, ensuring uniform dispersion and strong integration within the selective layer. This dual anchoring improves MOF-polymer adhesion, ensures uniform dispersion, and prevents delamination and defects in the selective layer.

CONCLUSION

UiO-66-2 NH_2 had been introduced to modify the polyamide rejection layer of the TFC membrane. Optimal integration of UiO-66-2 NH_2 into the polyamide layer led to a notable increase in water permeability, achieving a value of 3.40 l/m^2/h/bar. Additionally, salt rejection improved marginally from 97.6% to 99.0%. These superior permeability and desalination performances are attributed to two intrinsic UiO-66-2 NH_2 properties: (1) hydrophilic $-NH_2$ groups enhance water affinity of polyamide rejection layer via hydrogen bonding, lowering interfacial resistance and accelerating hydration; (2) uniform microporosity, which provides low-resistance water transport pathways within polyamide rejection layer. However, beyond optimal loading, nanoparticle aggregation and separation layer thickening increase mass transfer resistance, reducing water flux of TFC membrane.

Future work should focus on three priorities: (1) assessing membrane stability during extended operation under industrially relevant stressors-including fluctuating pH, chlorine exposure, and organic/inorganic fouling; (2) search for new characterization methods to conduct quantitative analysis of the defect distribution within the TFC membrane; and (3) performing long-term real-feed filtration tests with in-situ monitoring to identify the primary cause of flux and selectivity loss-mechanical compaction, pore narrowing, or polymer hydrolysis.

Acknowledgements: This study was supported by funding from "National & Local Joint Engineering Research Center for Mineral Salt Deep Utilization (SF202417)".

REFERENCES

1. Chung TS, Zhao D, Gao J, Lu K, Wan C, Weber M, Maletzko C (2019) Emerging R&D on membranes and systems for water reuse and desalination. *Chin J Chem Eng* **27**, 1578–1585.
2. Chu CH, Wang C, Xiao HF, Wang Q, Yang WJ, Liu N, Ju X, Xie JX, et al (2020) Separation of ions with equivalent and similar molecular weights by nanofiltration: sodium chloride and sodium acetate as an example. *Sep Purif Technol* **250**, 117199.
3. Loosdrecht MC, Brdjanovic D (2014) Anticipating the next century of wastewater treatment. *Science* **344**, 1452–1453.
4. Subramani A, Jacangelo JG (2015) Emerging desalination technologies for water treatment: A critical review. *Water Res* **75**, 164–187.

5. Tang CY, Yang Z, Guo H, Wen JJ, Nghiem LD, Cornelissen E (2018) Potable water reuse through advanced membrane technology. *Environ Sci Technol* **52**, 10215–10223.
6. Park HB, Kamcev J, Robeson LM, Elimelech M, Freeman BD (2017) Maximizing the right stuff: The trade-off between membrane permeability and selectivity. *Science* **356**, eaab0530.
7. Liang F, Liu D, Dong S, Zhao J, Cao X, Jin W (2022) Facile construction of polyzwitterion membrane via assembly of graphene oxide-based core-brush nanosheet for high-efficiency water permeation. *J Membr Sci* **644**, 120150.
8. Górecki R, Reurink DM, Khan MM, Sanahuja-Embuena V, Trzaskuś K, Hélix-Nielsen C (2020) Improved reverse osmosis thin film composite biomimetic membranes by incorporation of polymersomes. *J Membr Sci* **593**, 117392.
9. Shen J, Liu G, Han Y, Jin W (2021) Artificial channels for confined mass transport at the sub-nanometre scale. *Nat Rev Mater* **6**, 294–312.
10. Kadhom M, Deng B (2018) Metal-organic frameworks (MOFs) in water filtration membranes for desalination and other applications. *Appl Mater Today* **11**, 219–230.
11. Xiao F, Cao M, Chen Y (2024) UiO-66-$(OH)_2$-mediated transition layer for ultra-thin homogeneous defect-free polyamide membrane. *Surf Interf* **44**, 103607.
12. Zhao B, Sun M, Guo Z, Wang L, Qian Y, He X, Li J (2023) Enhanced water permeance and EDCs rejection using a UiO-66-NH_2-predeposited polyamide membrane. *Chemosphere* **312**, 137114.
13. Cavka JH, Jakobsen S, Olsbye U, Guillou N, Lamberti C, Bordiga S, Lillerud KP (2008) A new zirconium inorganic building brick forming metal organic frameworks with exceptional stability. *J Am Chem Soc* **130**, 13850–13851.
14. Rego RM, Kurkuri MD, Kigga M (2022) A comprehensive review on water remediation using UiO-66 MOFs and their derivatives. *Chemosphere* **302**, 134845.
15. Zhao DL, Yeung WS, Zhao Q, Chung TS (2020) Thin-film nanocomposite membranes incorporated with UiO-66-NH_2 nanoparticles for brackish water and seawater desalination. *J Membr Sci* **604**, 118039.
16. Liu H, Zhang M, Zhao H, Jiang Y, Liu G, Gao J (2020) Enhanced dispersibility of metal-organic frameworks (MOFs) in the organic phase via surface modification for TFN nanofiltration membrane preparation. *RSC Adv* **10**, 4045–4057.
17. Huo X, Jing Z, Wang H, Chang N (2022) Sodium dodecyl sulfate/C-UIO-66 regulation of nanofiltration membrane with pleated and thin polyamide layer structure. *Desalination* **538**, 115927.
18. Jayaramulu K, Horn M, Schneemann A, Saini H, Bakandritsos A, Ranc V, Petr M, Stavila V, et al (2021) Covalent graphene-MOF hybrids for high-performance asymmetric supercapacitors. *Adv Mater* **33**, 2004560.
19. Li S, Sun H, Huang Q, Xie X, Liu F (2025) Fabrication of UiO-66-F_4/TFC membranes for desalination. *Mater Lett* **382**, 137873.
20. Kalaj M, Denny Jr MS, Bentz KC, Palomba JM, Cohen SM (2019) Nylon–MOF composites through postsynthetic polymerization. *Angew Chem Int Ed* **58**, 2336–2340.
21. Cui X, Kong G, Wei S, Zhang Z, Kang Z, Guo H (2024) PolyMOF interlayers modulated interfacial polymerization of ultra-thin nanofiltration membranes with efficient and stable desalination performance. *J Membr Sci* **702**, 122780.
22. Zhang X, Zhang Y, Wang T, Fan Z, Zhang G (2019) A thin film nanocomposite membrane with pre-immobilized UiO-66-NH_2 toward enhanced nanofiltration performance. *RSC Adv* **9**, 24802–24810.
23. Tang P, Wang R, Chen Z (2018) In situ growth of Zr-based metal-organic framework UiO-66-NH_2 for open-tubular capillary electrochromatography. *Electrophoresis* **39**, 2619–2625.
24. Zhu J, Hou J, Yuan S, Zhao Y, Li Y, Zhang R, Tian M, Li J, et al (2019) MOF-positioned polyamide membranes with a fishnet-like structure for elevated nanofiltration performance. *J Mater Chem A* **7**, 16313–16322.
25. Kwon YN, Leckie JO (2006) Hypochlorite degradation of crosslinked polyamide membranes: II. Changes in hydrogen bonding behavior and performance. *J Membr Sci* **282**, 456–464.
26. Skrovanek DJ, Howe SE, Painter PC, Coleman MM (1985) Hydrogen bonding in polymers: infrared temperature studies of an amorphous polyamide. *Macromolecules* **18**, 1676–1683.
27. Wu ZW, Zeng JX, Yuan ZQ, Zhang R, Huang XP, Feng F, Chen MJ, Jin K, et al (2023) Polyamide/UiO-66-NH_2 nanocomposite membranes by polyphenol interfacial engineering for molybdenum(VI) removal. *Desalination* **563**, 116716.
28. Wu S, Zheng G, Lian H, Xing J, Shen L (1996) Chlorination and oxidation of aromatic polyamides. I. Synthesis and characterization of some aromatic polyamides. *J Appl Polym Sci* **61**, 415–420.
29. Kadhom M, Hu W, Deng B (2017) Thin film nanocomposite membrane filled with metal-organic frameworks UiO-66 and MIL-125 nanoparticles for water desalination. *Membranes* **7**, 31.
30. Ghanbari M, Emadzadeh D, Lau WJ, Matsuura T, Ismail AF (2015) Synthesis and characterization of novel thin film nanocomposite reverse osmosis membranes with improved organic fouling properties for water desalination. *RSC Adv* **5**, 21268–21276.